

Robust Control Strategy for Robotic Motorcycle Without Falling Down at Low-Speed Driving

Mitsuo Tsuchiya Susumu Hara Tetsuya Kimura Nao Tsurumi

本稿は、公益社団法人 日本自動車技術会 International Journal of Automotive Engineering 13 巻 (4) 頁: 188-195 2022 年11月に掲載された論文を同会の許可を得て転載したものです。本論文の著作権は公益社団法人 日本自動車技術会に属し、無断複製・転載を禁じます。

要旨

本稿では、自動二輪車の静止状態や低速走行中の安定性向上に関するロバスト制御について論じる。著者らは車両の重心位置を変更できる新しい回転軸を組み込んだロボットバイクを開発し、一般的な PID 制御器と単純な最適レギュレータを使用した制御の実証について報告した。さらに、マルチボディダイナミクス手法を用いてロボットバイクの数学モデルも導出し、そのモデルに最適レギュレータを適用した。しかし、実用化に向けた頑健な制御戦略に基づく実証実験はまだ行われていない。そこで本研究では実際の使用環境におけるロバスト性を実現するため、スライディングモードコントローラ (SMC) を適用した実用的な手法を提案する。それは、マイナー PID 制御ループと SMC を含む新しい数学モデルと周波数成形最適レギュレータによって設計された超平面を組み合わせた制御システム設計である。最後に、実際のロボットバイクを用いた実験によりその有効性を検証する。

Abstract

This study discusses robust control problems related to the fall of two-wheel motor vehicles during parking or low-speed driving. The robotic motorcycle includes a new rotary axis that can vary the position of the total center of gravity. Some authors have already reported preliminary control demonstrations using a typical PID controller and simple LQR. Moreover, the mathematical model of a robotic motorcycle derived using multibody dynamics methods and its optimal regulator simulation were developed. However, an experimental investigation of a robust control strategy for practical implementation has not yet been conducted. Therefore, this study proposes a practical method based on applying a sliding mode controller (SMC) to improve robust stability in a real usage environment. Here, we introduce the control system design combining a novel mathematical model, including a minor PID control loop and the SMC, with its hyperplane designed by the frequency-shaped optimal regulator. Finally, its effectiveness is verified by experiments using an actual robotic motorcycle.

1

INTRODUCTION

The automation of motorcycles from a vehicle and infrastructure perspective is essential. However, the term “vehicle” mainly refers to four-wheeled automobiles, and two-wheeled motorcycles are rarely the research focus. While many drivers enjoy driving a motorcycle itself, it is also a crucial mobility element in several countries, where riders use it for commuting and physical distribution because motorcycles are lighter and more compact than cars. Nevertheless, although they self-stabilize after gaining a certain speed, they are essentially unstable as an inverted pendulum while stationary or

during low-speed driving, which is a primary problem. Moreover, the rider must support considerable loads. Therefore, instability-related problems may become even more evident as the average age of motorcyclists increases, potentially slowing the development of a future mobile society centered on the autonomous driving of these systems.

In this regard, motorcycles must automatically self-stabilize in the parking state and during low-speed driving to counteract the weakness mentioned above. To achieve similar purposes, Ouchi et al. proposed a stabilization mechanism equipped with a gyro^[1], and

Satoh et al. developed a mechanism that stabilizes the vehicle by moving a counterweight in a direction orthogonal to its traveling direction^[2]. A study conducted by Saguchi et al. on a stabilization control method using steering is also well known^[3]. However, the method of Ouchi et al. often requires installing a relatively large and heavy gyro at a specific position to obtain a satisfactory result. Furthermore, the method of Satoh et al. widens the motorcycle; thus, losing the motorcycle the advantage of driving through narrow paths. In addition, riders have also pointed out that it is uncomfortable not to be able to lean motorcycles on curves. In contrast, the approach of Saguchi et al. is only practical while driving and cannot be applied while parked. The Honda Riding Assist developed by Araki et al. adopted a negative trail length and used steering to control the center of gravity in the stationary state^[4]. However, driving in the intended direction is challenging during extremely low-speed driving.

In 2017, the authors' company announced a robotic motorcycle equipped with an Active Mass Center Control System (AMCES) axis. This robotic motorcycle adds a rotation axis to increase the degree of freedom of the vehicle and allows self-balancing in an upright position by actively moving its entire mass center^[5]. Unlike other systems, the robotic motorcycle does not require large or heavy additional mechanisms and can remain stable, even in the stationary state. The demonstration of its capacity to drive at low speed and stabilize on its own was highly praised at the Tokyo Motor Show 2017 and other trade fairs. However, the control method during the demonstration was not based on a thoroughly examined mathematical model. Instead, the stabilization was achieved through the application of a proportional-integral-derivative (PID) control and an optimal linear quadratic regulator (LQR) tuned by trial and error^[5]. From the safety improvement perspective, motorcycles must become more reliable through more accurate and transparent modeling with a control system design method that better suits this problem, rather than a simple application of PID and LQR controls. With this objective in mind, Hara et al. attempted to model a

robotic motorcycle using a multibody dynamic system, which systematically modeled a complex, actual robotic motorcycle. The authors also demonstrated through numerical simulation that this motorcycle could be controlled satisfactorily by applying an optimal regulator based on the developed model^[6]. Nevertheless, the effectiveness of this model and its robustness to withstand actual conditions have not been verified empirically, and it has not been compared with the trial-and-error-based PID control of previous demonstrations.

Based on the above scenario, attempts have been performed to show experimentally that the robustness and stability of the robotic motorcycle can be improved and that it can serve as a vehicle to drive in actual traffic environments. However, previous studies have only implemented numerical simulations relying on a close-to-ideal problem setting^[7]. Moreover, ideal conditions do not necessarily apply when running in actual environments, and the road surface affects motorcycle driving. Therefore, to achieve robust self-stabilization in actual environments, this study mainly focused on self-stabilization during a stationary state or during low-speed driving. In this regard, we introduced a sliding mode controller (SMC) with a frequency shaper. And its effectiveness was experimentally demonstrated. The SMC considered the effect of structured and unstructured uncertainties and disturbances.

The structure of this paper is as follows. Section 2 describes the robotic motorcycle. In Section 3, previously presented modeling methods are discussed. In addition, the modeling of the control system, including the minimum PID control required for stabilization, is introduced. In Section 4, a practical control system design method that considers the proposed robust stabilization is described. The effectiveness of the proposed control system design method is demonstrated in Section 5 by analyzing the results of a numerical simulation and self-stabilization experiment during low-speed driving of an actual robotic motorcycle. Finally, in Section 6, the conclusions and further aspects are summarized.

2 THE ROBOTIC MOTORCYCLE WITHOUT FALLING DOWN

The robotic motorcycle (Fig. 1) is an experimental electric motorcycle^[5]. The most characteristic item is its rotating AMCES axis (Fig. 2). It runs through the center of the vehicle to control its center of gravity. The AMCES electronically controls and stabilizes the chassis of two-wheeled motorcycles. An optimal attitude can be maintained by controlling the chassis itself. The attitude of the machine is controlled by rotating parts of the counterweights, such as the battery, swing arm, and rear wheel around the AMCES axis. The AMCES axis also connects the red part (Q1) and blue part (Q2) in Fig. 2. During rotation, the counterweight parts move either right or left, enabling the machine to balance and remain upright. The intersection point of the AMCES axis and ground coincides with the grounding point of the rear wheel. Therefore, the grounding point of the rear wheel is always fixed even if the AMCES axis is rotated. The inner frame unit rotates around the AMCES axis. A schematic of this characteristic is shown in Fig. 2.



Fig. 1 The robotic motorcycle with a rotating shaft

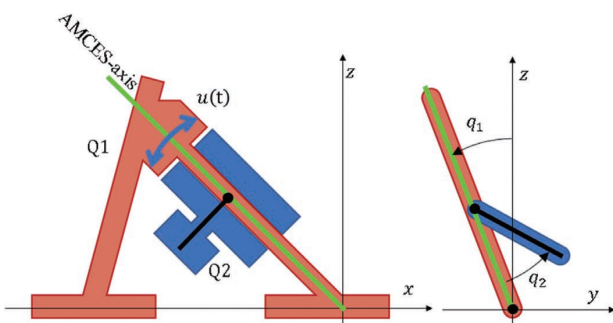


Fig. 2 Schematic figure of AMCES-axis

3 MATHEMATICAL MODELING

The mathematical modeling of the robotic motorcycle has already been investigated using multiple methodologies^{[6][7]}. The most important part of modeling is the AMCES axis. Therefore, the equation of motion for the robotic motorcycle was derived by introducing the following simplification to the system: The system is divided into two bodies (Fig. 2): a front-wheel and a rear-wheel parts. The AMCES shaft connects the bodies similar to a revolute joint. From the rear view of the main body, this mechanism can be regarded as a double pendulum. In addition, the system is considered a type of acrobot because only the connection portion of the body is actuated^[8].

After introducing the absolute coordinate system, the system is assumed to lie on flat ground. The x-axis is defined as the axis connecting the grounding points of the two tires. The z-axis is defined as being normal to the x-axis in the anti-gravity direction. The y-axis is defined as normal to the other axes based on the definition of the right-hand coordinate system. Here, the system differs from a typical acrobot because the directions of the x-axis and the AMCES axis are not similar. Therefore, the equation of motion cannot be simply described on a two-dimensional plane, and a particular modeling strategy is required. The front-wheel part of the motorcycle is defined as Q1, and the rear part is defined as Q2. Let q_1 be the slant angle of Q1 in the stationary state, and q_2 be the angle between Q1 and Q2 due to the rotation of the AMCES axis.

Two modeling methods were adopted in previous studies to obtain a linear approximated model of the robotic motorcycle. One method relies on Lagrange's equation of motion^[7]. This is a well-known modeling method based on Lagrangian mechanics^[9]. The second method relies on multibody dynamics^{[6][10][11]}. The results of the two methods are the same. The details can be found in previous papers^{[6][7]}. The approximated model is determined as follows:

$$\begin{aligned} \dot{x}(t) &= A_m x(t) + b_m u(t), \\ x(t) &= [q_1(t) \quad \dot{q}_1(t) \quad q_2(t) \quad \dot{q}_2(t)]^T, \end{aligned} \quad (1)$$

where $q_1(t)$ and $q_2(t)$ are the angles in Fig. 2, and $u(t)$ is the control input. More importantly, the safety of the experiments should be guaranteed. Thus, the robotic motorcycle requires a minor feedback loop to stabilize it in the control and the waiting modes. Its feedback gain vector k_m was selected via trial and error by stabilizing the vehicle during the waiting mode. In this regard, the single-input linearized controlled object model, including minor feedback control, is defined as follows:

$$\begin{aligned} \dot{x}_p(t) &= A_p x_p(t) + b_p u(t), \\ x_p(t) &= [q_1(t) \quad \dot{q}_1(t) \quad q_2(t) \quad \dot{q}_2(t)]^T, \end{aligned} \quad (2)$$

where $A_p = A_m - b_m k_m$ and $b_p = b_m$. Hereafter, the system in Eqs. (2) is referred to as the controlled object model. To identify the elements in A_p and b_p , the ARX model is applied to a real motorcycle under the M-sequence APRBS signal disturbance torque for $u(t) = u_d(t)$, as shown in Fig. 2. The details of the identification results can be found in our previous study^[12].

4 CONTROL SYSTEM DESIGN

4.1. Frequency-shaped LQ control hyperplane design for the controlled object model including the minor feedback

In contrast to previously published studies^{[5]-[7]}, the objective of this study is to achieve robust self-stabilization of a real robotic motorcycle in actual environments. In such a situation, the effects of uncertainties and disturbances cannot be ignored. As previously pointed out^[12], a real robotic motorcycle includes unstructured uncertainties such as high-order dynamics. The effect of high-order dynamics is reduced in this study by adopting a frequency-shaped optimal regulator (frequency-shaped LQ regulator, FSLQ) to reduce the control input signal in the high-frequency range^[13]. If low-speed driving is also considered, the influence of structured uncertainties, such as mass variations, must be handled more aggressively. To reduce the effect of both uncertainties simultaneously, this study adopts SMC using the FSLQ-control-based hyperplane design^[14]. SMC effectively reduce the effects of structural uncertainties, such as parameter variations and disturbances, such as Coulomb friction (the disturbances

that meet the matching condition). Moreover, we discuss an appropriate SMC design method for this control problem.

For the FSLQ regulator design, the second-order Butterworth low-pass characteristic with a cutoff frequency of 5 Hz on the control input is applied. Its dynamic characteristics are determined using the following state equation:

$$\begin{aligned} \dot{x}_f(t) &= A_f x_f(t) + b_f u_a(t), \quad u_f(t) = c_f x_f(t) \\ A_f &= \begin{bmatrix} 0 & 1 \\ -\omega_f^2 & -2\zeta_f \omega_f \end{bmatrix}, \quad b_f = \begin{bmatrix} 0 \\ \omega_f^2 \end{bmatrix}, \quad c_f = [1 \quad 0], \end{aligned} \quad (3)$$

where ω_f and ζ_f are the cutoff frequency (5 Hz) and damping ratio ($1/\sqrt{2}$: Butterworth type), respectively. Subsequently, the feedback control system obtained using the LQ control feedback gain vector $k_a = [k_p \quad k_f]$ for the augmented system is expressed as follows:

$$\begin{aligned} \dot{x}_a(t) &= A_a x_a(t) + b_a u_a(t), \\ u_a(t) &= -k_p x_p(t) - k_f x_f(t) = -k_a x_a(t) \\ x_a(t) &= \begin{bmatrix} x_p(t) \\ x_f(t) \end{bmatrix}, \quad A_a = \begin{bmatrix} A_p & b_p c_f \\ 0 & A_f \end{bmatrix}, \quad b_a = \begin{bmatrix} 0 \\ b_f \end{bmatrix}. \end{aligned} \quad (4)$$

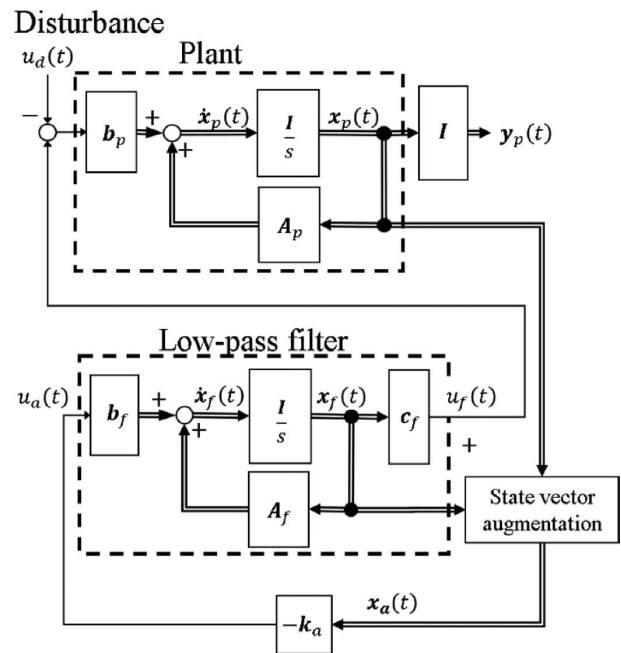


Fig. 3 Block diagram of the FSLQ control system

The block diagram of the FSLQ regulator is shown in Fig. 3. The hyperplane distance $\sigma(t)$ for SMC in this study was designed using Eqs. (4), as follows:

$$\sigma(t) = s_a x_a(t), \quad (5)$$

where s_a is a linear operator and is set to the optimal feedback gain vector k_a of the LQ control solution of the augmented system in Eqs. (4) and the appropriate weighting matrices Q_a and r_a . This procedure is similar to the hyperplane design method based on using the system zeros^[15].

4.2. Sliding mode control design

The SMC system design relied on a two-step design^[15]. The first step was the equivalent linear system design of the switching hyperplane. As the reference^[15], the eigenvalues of the equivalent linear system:

$$\dot{x}_a(t) = \left\{ A_a - b_a (s_a b_a)^{-1} s_a A_a \right\} x_a(t), \quad (6)$$

consists of five stable poles and one origin pole. The augmented system can be written as follows:

$$\begin{aligned} s_a &= [s_1 \quad s_2], \\ s_1 &= s_2 k_{ppm}, \\ \dot{x}_1(t) &= (A_{11} - A_{12} k_{ppm}) x_1(t), \\ x_1(t) &= [q_1(t) \quad \dot{q}_1(t) \quad q_2(t) \quad \dot{q}_2(t) \quad x_f(t)]^T, \\ A_{11} &= \begin{bmatrix} A_p & b_p \\ 0^{1 \times 4} & 0 \end{bmatrix}, A_{12} = \begin{bmatrix} 0^{4 \times 1} \\ 0 \end{bmatrix}, b_1 = \begin{bmatrix} 0^{4 \times 1} \\ 1 \end{bmatrix}, \\ A_{21} &= [0^{1 \times 4} \quad -\omega_f^2], A_{22} = [-2\zeta_f \omega_f], b_2 = [\omega_f^2]. \end{aligned} \quad (7)$$

The hyperplane normal vector s_a can be determined using k_{ppm} provided that $x_1(t)$ can be stabilized with s_2 as an arbitrary value other than zero. In this study, the equivalent control input $u_l(t)$ is derived from Eq. (8) for a constant hyperplane distance ($\sigma(t) = \text{const.}$) to obtain Eqs. (9), which corresponds to Eq. (6).

$$\dot{\sigma}(t) = s_a \dot{x}_a(t) = s_a (A_a x_a(t) + b_a u_a(t)) = 0. \quad (8)$$

$$u_l(t) = -k_a x_a(t),$$

$$k_a = (s_a b_a)^{-1} s_a A_a. \quad (9)$$

Equation (8) corresponds to the popular equivalent

control input in Eqs. (10) when the hyperplane distance is set to zero ($\sigma(t) \rightarrow 0$)^[15]. The control design using Eq. (8) generalizes the constraint of the state on the hyperplane and increases the design degrees of freedom.

$$\dot{x}_1(t) = (A_{11} - A_{12} k_{ppm}) x_1(t),$$

$$k_{ppm} = (s_2 b_2)^{-1} \left[(s_1 A_{11} + s_2 A_{21}) - (s_1 A_{12} + s_2 A_{22}) s_2^{-1} s_1 \right]. \quad (10)$$

The second step is a nonlinear control design to restrain the state of the switching hyperplane. A smoothing function is considered to obtain the following equation for the constrained control input (nonlinear feedback control input) $u_n(t)$ in the hyperplane^[15]:

$$u_n(t) = -\alpha \frac{\sigma(t)}{|\sigma(t)| + \varepsilon}, \quad (11)$$

where α and ε respectively represent the sliding mode control gain α [Nm], and the mitigation coefficient ε is introduced to suppress chattering. Moreover, $\sigma(t)$ based on Eq. (5) is the inner product of the hyperplane normal vector s_a and expanded state variable $x_a(t)$. Setting the sliding mode control gain α and the mitigation coefficient to suppress chattering ε enable the design of the nonlinear control input $u_n(t)$.

Figure 4 shows a block diagram summarizing the entire control system based on the proposed two-step design.

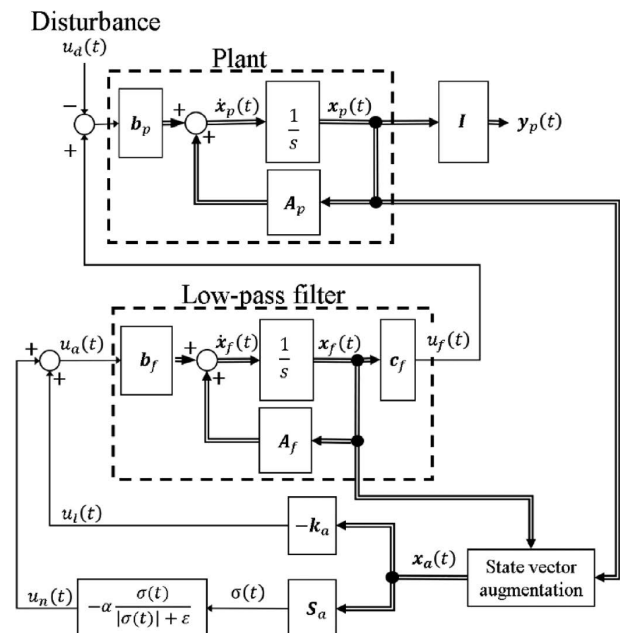


Fig. 4 Block diagram of the robust control system

The most important factor in FSLQ control is the fall prevention of the vehicle. Therefore, the weights were set only to the vehicle roll angle and its derivative. Even if the weights of the elements related to the AMCES angle and the frequency shaper element are set to 0, the purpose of the control, such as fall prevention and residual mode suppression, works well. The weight to the control input is set to 1, specifically, $Q_a = \text{diag}[1 \times 10^4 \ 1 \times 10^3 \ 0 \ 0 \ 0 \ 0]$, $r_a = 1$.

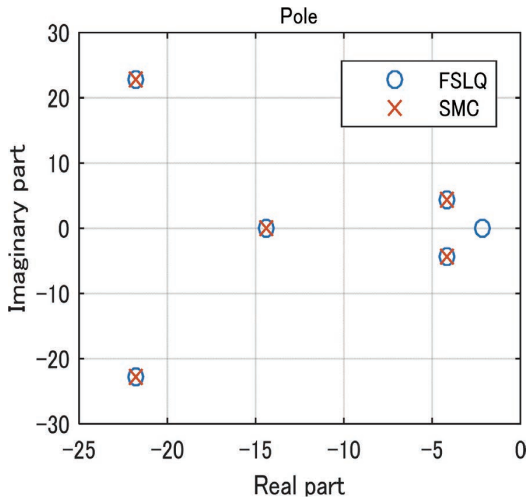


Fig. 5 FSLQ closed-loop poles and hyperplane design poles

For the hyperplane design of the SMC, we applied a pole placement design using five poles (Fig. 5) with the origin pole removed from the poles, including the feedback of the FSLQ control. s_2, k_{ppm} and $|s_a|$ in Eqs. (7) are 1, $[-1.3 \times 10^5 \ -2.7 \times 10^4 \ 2.4 \times 10^4 \ 3.1 \times 10^3 \ 4.8 \times 10^1]$ and 1.35×10^5 , respectively where $|s_a|$ is the hyper plane normal vector length. The equivalent control input $u_f(t)$ was used in Eqs. (9). The sliding mode control gain α of the nonlinear control input $u_n(t)$ was set to 500 Nm, approximately twice the maximum torque of the actuator at 298 Nm. The mitigation coefficient ε was set to 5.0×10^4 by trial and error, representing 37% of $|s_a|$. In this paper, we assumed the roll angle range and disturbance roll torque range in which the vehicle can avoid overturning. Accordingly, α and ε are adjusted so that the nonlinear control input becomes the maximum value of the actuator at the limited boundary. Large mitigation coefficient is also intended to suppress unmodeled higher-order vibration modes.

5 SIMULATIONS AND EXPERIMENTS

All simulations and experiments were performed using the same parameters. The sampling and control periods were set to 1.0 ms.

The simulation and experiment results were evaluated by applying two types of disturbances. Figure 6 shows an experiment simulating the left-right shift of the center of gravity of the rider. The disturbance was a bump disturbance where a maximum of 150 Nm was loaded on the AMCES shaft in 0.5 s and unloaded in 0.5 s, and $u_d(t) = 150 \cos^2(\pi t / 2)$.



Fig. 6 Experiment applying a disturbance to the AMCES shaft

Figure 7 shows an experiment simulating the effect of a crosswind with a wind speed of 6 m/s. A 5 kg weight was placed at the end of the handle. Hereafter, the experiment in Fig. 6 is referred to as disturbance(a), and the experiment in Fig. 7 is referred to as disturbance(b).



Fig. 7 Experiment applying a weight to the handle end

5.1. Simulations

Figure 8 shows the results for disturbance(a). The disturbance torque (black dashed line) to the AMCES axis was applied counterclockwise for 2 s after starting the experiment and clockwise 7 s later. With only minor loop control (blue one-dot chain line), there was no plant control input $u_r(t)$. The maximum roll angle is 2.50° , and the roll angle does not completely converge to the origin in 4 s. With FSLQ control (blue dashed line), the maximum plant control input is 71 Nm (47% compensation), the maximum roll angle is 1.45° (42% improvement), and the roll angle completely converges in 4 s. With SMC (solid red line), the maximum plant control input is 128 Nm (86% compensation), the maximum roll angle is 0.65° (74% improvement), and the roll angle completely converges within 4 s.

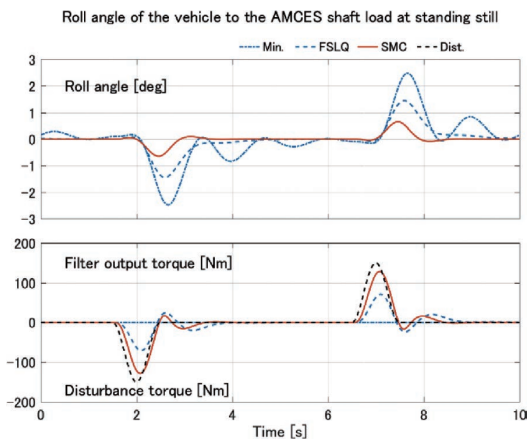


Fig. 8 Simulation of applying a bump disturbance to the AMCES shaft in the stationary state

Figure 9 shows the results of the disturbance(b). A 5 kg weight was placed at the end of the handle and stabilized with only minor loop control, and each control was started after 5 s. With FSLQ control, the improvement in the rolling angle is 0.21° (12.6% improvement). With the SMC, the improvement is 0.97° (58.5% improvement). In addition, SMC is 4.6 times better than the FSLQ control.

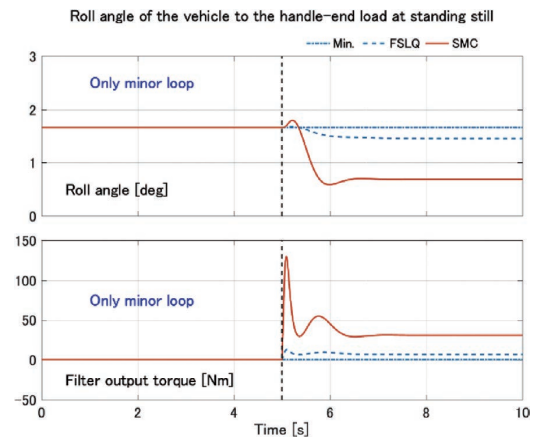


Fig. 9 Simulation of load at end of handle in the stationary state

Figure 10 shows the time transition of the state in SMC using a scatter diagram. The rolling angle and AMCES rotation angle (blue line), hyperplane (black dashed line), and hyperplane distance $\sigma(t)$ (red dashed line) are plotted. For the hyperplane, zeros were assigned to state variables other than the rolling angle and AMCES rotation angle. The state was controlled to approach the hyperplane immediately after starting the control and then to the origin.

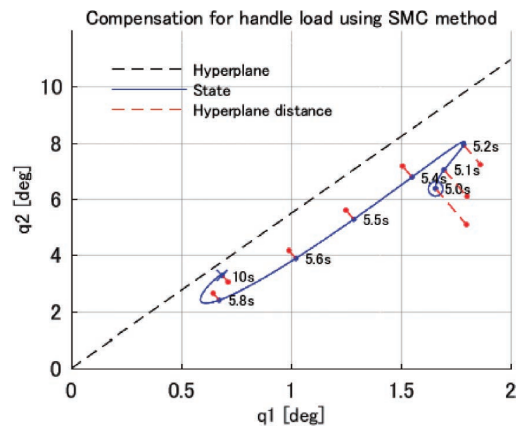


Fig. 10 Time transition of vehicle attitude with the handle-end load in SMC

Figure 11 details Fig. 10 and plots the roll angle, AMCES angle, frequency shaping control input, hyperplane distance, equivalent control input and nonlinear control input. At the start of control, the nonlinear control input acts more dominantly than the equivalent control input and the AMCES angle increases. After that, the vehicle roll angle decreases as the AMCES angle increases. The SMC compensates for the load on the handle end with a nonlinear control input that constrains the state variables to the hyperplane.

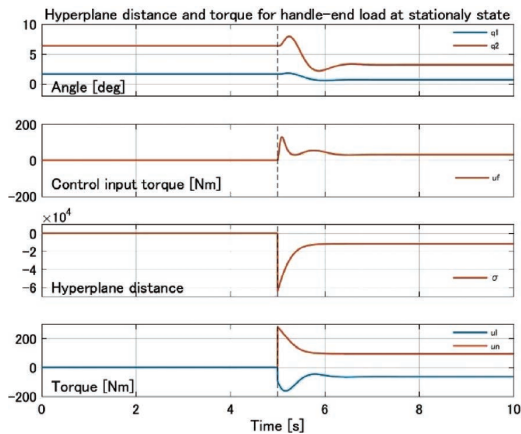


Fig. 11 Time series response in SMC to the handle-end load at stationary state: roll angle, AMCES angle, frequency shaping control input, hyperplane distance, equivalent control input and nonlinear control input

5.2. Experiments

In the stationary state, disturbance(a) and disturbance(b) were experimented. However, in the low-speed driving condition, only disturbance(a) was experimented.

5.2.1. Experiments on a vehicle stationary state

Figure 12 shows the experimental results for disturbance(a) in the stationary state. With only minor loop control, the maximum rolling angle is 2.2°, and the rolling angle does not converge to the origin in 4 s. In contrast, with FSLQ control, the maximum rolling angle is 1.1° (50% improvement), and the rolling angle converges to the origin in 4 s. With SMC, the maximum rolling angle is 0.6° (73% improvement), and the rolling angle converges to the origin in 4 s. For all controls, the simulation and experimental results shown in Fig. 7 were correlated.

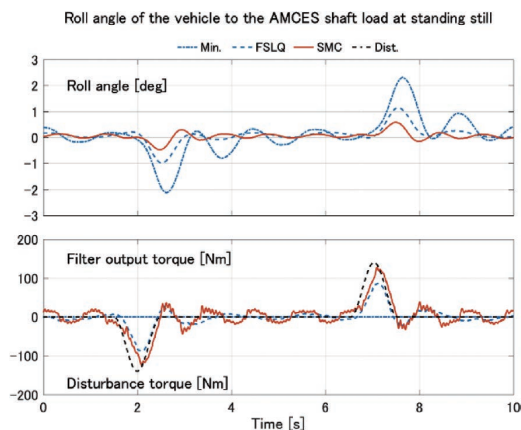


Fig. 12 Experiment involving applying a bump disturbance to the AMCES shaft at stationary state

Figure 13 shows the experimental results for disturbance(b) in the stationary state. With FSLQ control, almost no control input was required when the control was started, and the rolling angle hardly improved. With SMC, a control torque of 150 Nm was input at the start of the control, and the rolling angle improved by 50% in 1 s. Similar to the previous experiments, for all controls, the simulation and experimental results shown in Fig. 8 were correlated.

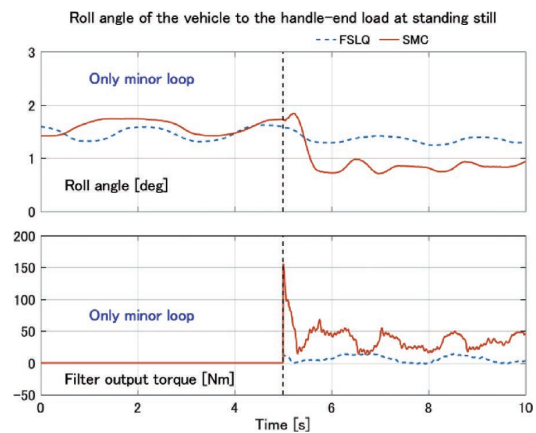


Fig. 13 Experiment involving applying a disturbance to the handle-end load at stationary state

5.2.2. Experiments on a vehicle low-speed driving

Figure 14 shows the experimental results for disturbance(a) during low speed straight driving at 0.5 km/h. With only a minor loop control, the maximum rolling angle was 2.9°, which was 32% lower than that of 2.2° in the stationary state. In addition, the convergence of the rolling angle owing to the disturbance was worse in low-speed driving than in the stationary state. This is because the AMCES structure and the driving force push the vehicle sideways. With the FSLQ control, the maximum rolling angle was 1.2° (58% improvement), but the rolling angle did not converge to the origin. With the SMC, the maximum rolling angle was 0.8° (72% improvement), and the rolling angle converged to the origin. The SMC estimated the disturbance more accurately than the FSLQ control, and the timing to start the compensation was earlier. The superiority of SMC over FSLQ control during low-speed driving tends to be the same as that in the stationary state.

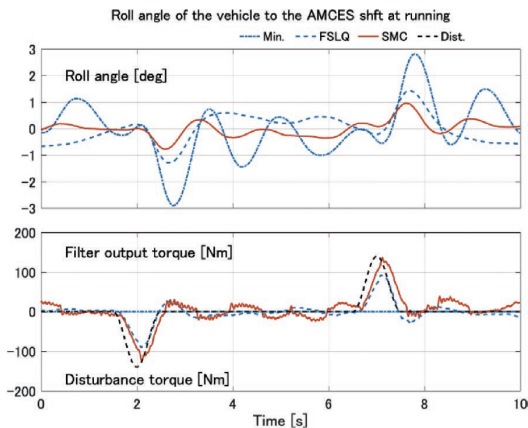


Fig. 14 Experiment results for bump disturbance applied during straight line low-speed driving

Figure 15 shows the time transition of the SMC during low-speed driving. As shown in the block diagram in Fig. 4, the sum $u_a(t)$ of the equivalent control input $u_l(t)$ and the nonlinear control input $u_n(t)$ is the input of the frequency shaper. The frequency shaper removes the high-frequency control input and becomes the plant control input $u_f(t)$. The $u_f(t)$ responded well to the applied torque disturbance $u_d(t)$, and $u_f(t)$ was highly correlated with $u_n(t)$. When the state began to be peeled off from the hyperplane by the applied disturbance torque, the compensation by the nonlinear control input $u_n(t)$ had already started, and the nonlinear control input $u_n(t)$ almost compensated the applied disturbance torque $u_d(t)$.

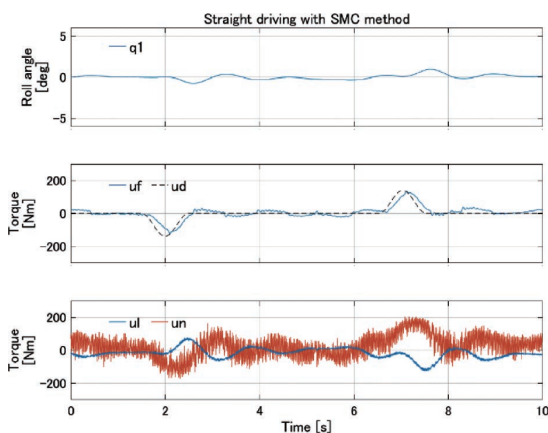


Fig. 15 Experiment results for bump disturbance applied during driving at a speed of 0.5 km/h

In addition to straight-line driving, only SMC permitted drive stably in a turning examination at a steering angle

of 30° (turning radius of 3 m) at a speed of 0.5 km/h. And the control input for bump disturbance of SMC was the same as in a straight-line driving^[16].

6 CONCLUSION

This paper introduced the robust control problem for a motorcycle without falling to a new mobility system. Improving motorcycles in a stationary state or during low-speed driving is a non-negligible factor for future mobile societies. Moreover, how to ensure low-speed driving stability using the robotic motorcycle was discussed. This motorcycle is equipped with a new axis of rotation named AMCES and can change the position of the total center of gravity. We developed a system model that included stabilizing the PID control, as previously demonstrated. In addition, a sliding mode controller (SMC) with a frequency-shaped optimal regulator (FSLQ) was developed to suppress the effects of structural and nonstructural uncertainties. The effectiveness of the developed approach was verified by a low-speed driving experiment using a real robotic motorcycle.

In the future study, the nonlinearity of the controlled object may be an important subject. When the vehicle stands up from the kickstand state, the AMCES axis rotates 50° . Centrifugal force due to vehicle speed cannot be ignored when turning. If the roll angle can be properly controlled, the performance of the vehicle dynamics will be improved even at low-speed driving.

ACKNOWLEDGMENTS

The authors would like to thank Mr. Eiichirou TSUJII for his valuable contributions to the robotic motorcycle project.

REFERENCES

- [1] Ouchi, S., Kodani, N., Hirata, H., Takahashi, K. and Chida, Y., Self-sustaining driving control of two-wheeled vehicle by using gyro-actuator, Transactions of the Japan Society of Mechanical Engineers (in Japanese), Vol. 81, No. 832 (2015), 15-00207.

[2] Satoh, H. and Namerikawa, T., Modeling and robust attitude control of stationary self-sustaining two-wheeled vehicle, Transactions of the Japan Society of Mechanical Engineers Part C, Vol. 72, No. 719 (2006), pp. 2130-2136 (in Japanese).

[3] Saguchi, T., Yoshida, K. and Takahashi, M., Stable running control of autonomous bicycle robot, Transactions of the Japan Society of Mechanical Engineers Part C, Vol. 73, No. 731 (2007), pp. 2036-2041 (in Japanese).

[4] Araki, M., Akimoto, K. and Takenaka, T., Study of riding assist control enabling self-standing in stationary state, SAE International Journal of Vehicle Dynamics, Stability, and NVH, Vol. 3, No. 1 (2019), pp. 47-56.

[5] Tsujii, E., Tsuchiya, M., Terayama, T. and Tsurumi, N., Study on self-standing motorcycle control mechanism, Transactions of Society of Automotive Engineers of Japan, Vol. 50, No. 4 (2019), pp. 1049-1054 (in Japanese).

[6] Hara, S., Nakagami, K., Miyata, K., Tsuchiya, M. and Tsujii, E., Dynamics and control of self-standable motorcycle, Proceedings of the ASME 2019 International Design Engineering Technical Conferences and Computers and Information in Engineering Conference, (2019), DETC2019-97154.

[7] Hara, S., Nakagami, K., Miyata, K., Tsuchiya, M. and Tsujii, E., Robust control system design for self-standable motorcycle, Journal of Advanced Mechanical Design, Systems, and Manufacturing, Vol. 14, No. 3 (2020), JAMDSM0030.

[8] Spong, M. W., The swing up control problem for the Acrobot, IEEE Control Systems, Vol. 15, No. 1 (1995), pp. 49-55.

[9] Taylor, J. R., Classical Mechanics (2005), University Science Books.

[10] The Japan Society of Mechanical Engineers ed., Multibody Dynamics (1) –Fundamental Theory– (2006), Corona Publishing (in Japanese).

[11] The Japan Society of Mechanical Engineers ed., Multibody Dynamics (2) –Numerical Analysis and Applications– (2007), Corona Publishing (in Japanese).

[12] Tsuchiya, M., Hara, S., Nakagami, K., Tsurumi, N. and Kimura, T., Optimal control experiment of self-standable motorcycle MOTOROiD, Proceedings of the SICE Annual Conference 2020, (2020), pp. 1324-1328.

[13] Kida, T., Ikeda, M. and Yamaguchi, I., Optimal

regulator with low-pass property and its application to LSS control, Transactions of the Society of Instrument and Control Engineers, Vol. 25, No. 4 (1989), pp. 448-454 (in Japanese).

[14] Ito, T. and Nonami, K., Sliding mode control with frequency shaping to suppress spillover, Transactions of the Japan Society of Mechanical Engineers Series C, Vol. 63, No. 611 (1997), pp. 2308-2314 (in Japanese).

[15] Nonami, K., Nishimura, H. and Hirata, M., Control Systems Design by MATLAB (1998), Tokyo Denki University Press, pp. 163-201 (in Japanese).

[16] Hara, S., Tsuchiya, M. and Kimura, T., Robust control of automatic low-speed driving motorcycle “MOTOROiD”, Proceedings of the 2021 IEEE 10th Global Conference on Consumer Electronics (2021), pp.724-725.

■ 著者



土屋 光生
Mitsuo Tsuchiya
技術・研究本部
技術開発統括部
制御システム開発部



原 進
Susumu Hara
名古屋大学
大学院工学研究科
航空宇宙工学専攻 教授



木村 哲也
Tetsuya Kimura
技術・研究本部
NV・技術戦略統括部
技術戦略部
※執筆時



鶴見 尚
Nao Tsurumi
技術・研究本部
技術開発統括部
制御システム開発部